Digest Journal of Nanomaterials and Biostructures

Dig. J. Nanomater. Bios. **2026**; 21(3): 52488
https://doi.org/10.31083/DJNB52488

Original Research

Salt- and Temperature-Responsive Poly(ethyleneimine)/Phenylthioacetic Acid Ion-Pair Assemblies

Jeong Seon Hwang[1,†], Wenting Long[1,†], Jin-Chul Kim[1,*]

[1]Department of Biomedical Science & Institute of Bioscience and Biotechnology, Kangwon National University, 24341 Chuncheon, Gangwon, Republic of Korea

*Correspondence: jinkim@kangwon.ac.kr (Jin-Chul Kim)

[†]These authors contributed equally.

Academic Editor: Karol Kyzioł

Submitted: 1 April 2026 Revised: 9 June 2026 Accepted: 15 June 2026 Published: 14 September 2026

Abstract

Background: BackgroundIon pairs formed through electrostatic attraction between poly(ethyleneimine) (PEI) and phenylthioacetic acid (PTA) underwent self-assembly in aqueous solution. This interaction, and consequently the structural stability of the ion-pair self-assemblies (IPSAMs), can be affected by salt ions present in the body (e.g., Na^+ and Ca^{2+}) through charge screening or competitive interactions. Therefore, the prepared IPSAMs were expected to exhibit salt-responsive behavior. IPSAMs can undergo phase transitions following ion-pair formation, suggesting that temperature-dependent and salt-responsive release behavior may also occur. **Methods:** IPSAMs were prepared at PEI/PTA molar ratios of 3/7, 4/6, 5/5, 6/4, and 7/3, and their phase transition temperatures were measured to select a representative formulation. The selected IPSAM was treated with NaCl and $CaCl_2$, and the resulting structural changes were evaluated using instrumental (Fourier transform infrared spectroscopy, surface tension, particle size, zeta potential, and transmission electron microscopy) analyses. Nile Red was used as a model hydrophobic compound to investigate release behavior under different temperature and salt conditions. **Results:** Among the prepared formulations, IPSAM(3/7) exhibited an upper critical solution temperature of 38.37 °C, which is remarkably close to the human body's fever threshold and active metabolic states. Therefore, IPSAM(3/7) showed potential as a tunable bioswitch capable of operating under physiologically relevant thermal conditions and was selected as a representative formulation for further experiments. After salt treatment, the phase transition temperature of this IPSAM decreased. Instrumental analyses confirmed that salt treatment reduced the colloidal stability of the IPSAM and induced structural changes. $CaCl_2$ showed a greater effect than NaCl, which suggests that compared with Na^+ ions, Ca^{2+} ions more strongly perturbed the PEI/PTA ion-pair structure through their stronger charge screening effect and, possibly, interactions with carboxylate groups. Nile Red release experiments confirmed the salt-responsive and temperature-responsive release behavior of IPSAMs. **Conclusions:** The developed PEI/PTA IPSAM can function as a stimulus-responsive nanocarrier responding to both temperature and ionic conditions. The proximity of the phase transition temperature of IPSAM(3/7) to a physiologically meaningful temperature range supports its potential application as a tunable bioswitch for targeted delivery.

Keywords: ion pair self-assembly; salt responsiveness; temperature responsiveness; phenylthioacetic acid; poly(ethyleneimine)

1. Introduction

Stimulus-responsive nanocarriers have attracted considerable attention as drug delivery carriers that release payloads in response to specific environmental triggers, thereby reducing nonspecific distribution and associated side effects. In addition to the tumor microenvironment (TME) and other pathological conditions, physiological environments containing various salts, such as the skin, mucosal tissues, wound sites, and body fluids, can also provide useful ionic cues for responsive drug release. Salt-responsiveness is particularly relevant in these environments because the skin is continuously exposed to sweat containing NaCl, mucosal tissues are covered with electrolyte-containing mucus, and wound sites produce exudates rich in salts and proteins. At wound sites, the ionic composition of exudates can also change during inflammation and healing as tissue fluid leakage, cellular activity, and tissue repair proceed. Therefore, local salt conditions in these tissues may weaken the electrostatic ion pair interactions that maintain ion pair self-assembly (IPSAM) stability, induce structural destabilization, and promote drug release at the target site. In such environments, salts such as NaCl and $CaCl_2$ are abundantly present and may induce structural changes or collapse of nanocarriers through competitive ionic interactions with external ions [1,2,3,4,5]. Researchers have investigated various stimulus-responsive drug delivery carriers, including liposomes, micelles, cubosomes, nanofibers, nanoparticles, and microparticles [6,7,8,9,10]. Among them, micelles are self-assembled structures formed by amphiphilic molecules in aqueous solution and offer advantages such as relatively simple preparation and efficient encapsulation of hydrophobic drugs [11,12,13,14,15]. Micelles are generally prepared using amphiphilic materials such as surfac-

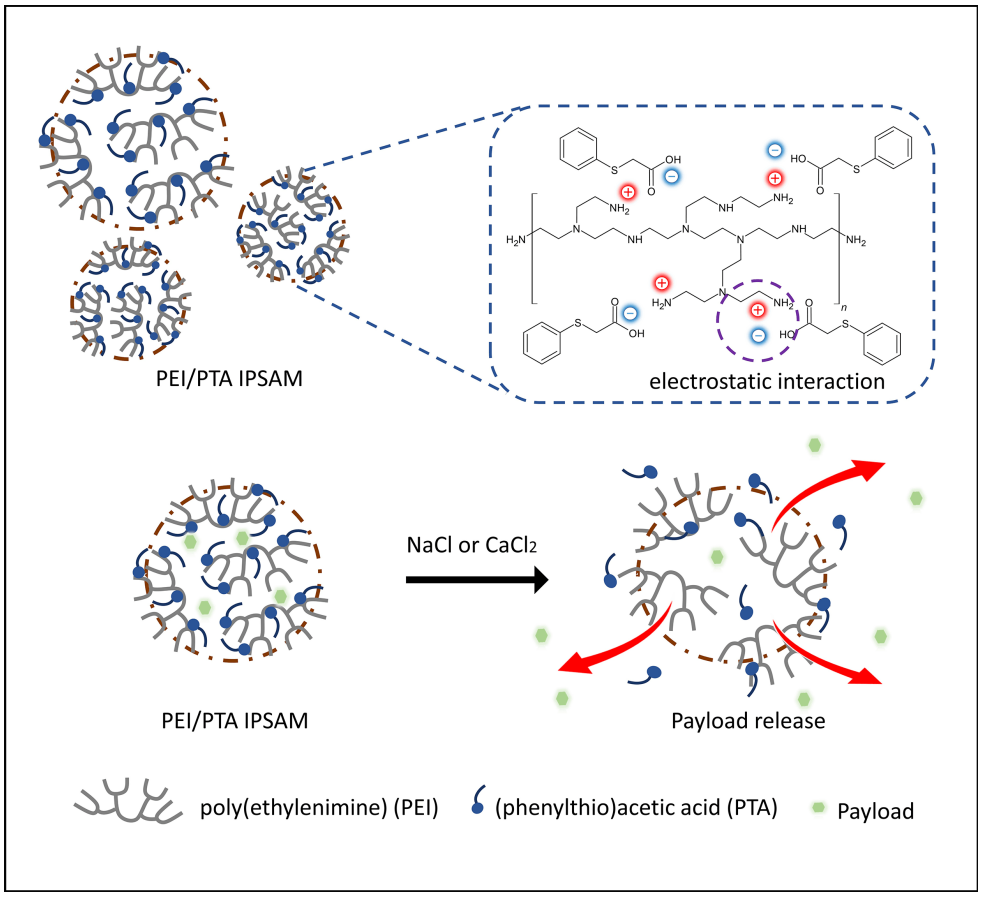

Scheme 1. Schematic representation of payload release from PEI/PTA IPSAM triggered by NaCl or $CaCl_2$ through disruption of ion pair interactions. PEI, poly(ethyleneimine); PTA, phenylthioacetic acid; IPSAM, ion pair self-assembly.

tants or block copolymers. More recently, however, studies have also explored the formation of nanocarriers based on amphiphilicity induced by ionic interactions [16,17]. IPSAM forms through electrostatic interactions between a hydrophilic cationic polymer and a hydrophobic counterion. Specifically, when ion pairs are formed between the amine groups of the polymer and the negatively charged functional groups of the counterion, the resulting complex exhibits an amphiphilic structure possessing both hydrophilic and hydrophobic characteristics. These amphiphilic ion pairs can spontaneously self-assemble in aqueous solution to form micelles. This approach offers the advantage of producing micelles in a relatively simple manner while minimizing the need for complex covalent synthesis and multistep purification processes. In addition, IPSAM is sensitive to external ionic environments. For example, in the presence of salts such as NaCl or $CaCl_2$, external ions can interfere with the existing ion pair interactions, thereby weakening the ion pair binding strength or reducing the structural stability of the micelles. These changes may induce the collapse of the micelles, ultimately leading to the release of the loaded drug [18,19,20]. Previous studies reported poly(ethyleneimine) and phenylthioacetic acid-based ion pair self-assembly (IPSAM) as a stimulus-responsive nanocarrier showing temperature- and reduction-responsive behavior. poly(ethyleneimine) (PEI)/phenylthioacetic acid (PTA) IPSAM was previously shown to interact with KB cells and undergo cellular internalization, as confirmed by confocal laser scanning microscopy [16]. In addition, another IPSAM formulation was reported to retain its carrier function *in vivo* and accumulate at tumor sites, as demonstrated by confocal imaging and *in vivo* imaging system (IVIS) imaging in animal models [21]. These findings suggest that IPSAM can retain its function as a nanocarrier not only in simple buffer media but also in cellular and *in vivo* environments, supporting its potential use as a drug carrier for cancer-related applications. However, the response of PEI/PTA IPSAM to NaCl and $CaCl_2$ under physiologically relevant salt conditions has not been fully examined. Since external ions such as NaCl and $CaCl_2$ can competitively interfere with ion pair interactions, salt-rich environments may significantly affect the structural stability and drug release behavior of IPSAM. Therefore, in this study, we investigated the salt-responsive behavior of PEI/PTA IPSAM and evaluated its potential as a carrier for drug release in ionic physiological environments such as the skin, mucosal tissues, and body fluids (Scheme 1).

2. Materials and Methods

2.1 Materials

PTA, PEI, Tris buffer (Trizma base), NaCl, $CaCl_2$, and Nile red were purchased from Sigma-Aldrich (St. Louis, MO, USA). All chemicals were of analytical grade and used without further purification.

2.2 Preparation of PEI/PTA IPSAM(a/b)

PEI and PTA were mixed in 5 mL of Tris buffer (30 mM, pH 7.0) in 10 mL vials at different feed ratios. The final concentrations of both PEI and PTA were maintained at 20 mg/mL, while the molar ratios of amino groups to carboxyl groups were varied as 3/7, 4/6, 5/5, 6/4, and 7/3. The resulting dispersions were gently mixed on a roller mixer at room temperature for 12 h. The prepared formulations were denoted as IPSAM(a/b), in which a/b indicates the molar ratio of amino groups to carboxyl groups.

2.3 Determination of Upper Critical Solution Temperature

To evaluate the upper critical solution temperature of IPSAM, temperature-dependent transmittance was monitored at 600 nm using an ultraviolet–visible (UV–Vis) spectrophotometer equipped with a temperature control system (6505 UV/Vis Spectrophotometer, JENWAY, Stone, UK). IPSAM(a/b) samples were prepared at 20 mg/mL with amino-to-carboxyl molar ratios ranging from 3/7 to 7/3, and 1 mL of each sample was loaded into a 1.5 mL cuvette for analysis. During measurement, the temperature was raised from 20 to 50 °C at a constant rate of 2 °C/min while transmittance was continuously recorded. The upper critical solution temperature (UCST) was determined from the intersection between the baseline region showing nearly constant transmittance and the region where the transmittance started to increase. For the subsequent study, IPSAM(3/7) was selected and prepared as a 15 mL mother solution. Aliquots were then dispensed into 5 mL vials and adjusted to a final volume of 1 mL so that the final concentrations of NaCl and $CaCl_2$ were 0, 20, 30, 50, 100, and 150 mM, respectively. The UCST under these conditions was measured using the same procedure described above.

2.4 FT-IR Analysis

Fourier-transform infrared (FT-IR) spectroscopy was employed to analyze changes in the characteristic amino- and carboxyl-associated peaks after ion pair formation between PEI and PTA. PEI and IPSAM(a/b) solutions were prepared at 20 mg/mL in 30 mM Trizma buffer adjusted to pH 7.0, and 3 mL of each solution was transferred into Eppendorf tubes. For salt-treated conditions, NaCl and $CaCl_2$ were separately added to IPSAM(a/b) samples to final concentrations of 20 and 150 mM. The samples were frozen at –80 °C for 1 h, followed by freeze-drying for 48 h. After lyophilization, PEI, PTA, and IPSAM(a/b) samples were mixed with KBr, ground into a fine powder, and pressed into pellets prior to analysis. The infrared spectra were collected using an FT-IR spectrometer (FT-3000 Excalibur, Varian Inc. Palo Alto, CA, USA).

2.5 Surface Tension Measurement of IPSAM

Surface tension was measured to evaluate the amphiphilic characteristics of PEI, PTA, and IPSAM(a/b). All samples were prepared in 30 mM Trizma buffer at pH 7.0, and IPSAM formulations with amino-to-carboxyl molar ratios ranging from 3/7 to 7/3 were adjusted to 20 mg/mL in a final volume of 10 mL. Measurements were performed using a tensiometer (DST 60, SEO Co., Gunpo, South Korea) by the ring method. Following the initial measurement, each sample was serially diluted twofold, and surface tension was recorded after each dilution step until the values became close to that of pure water. For salt-treated conditions, IPSAM(3/7) was prepared with NaCl or $CaCl_2$ at final concentrations of 0, 20, 30, 50, 100, and 150 mM, with the total volume adjusted to 10 mL in each case. After gentle mixing, surface tension was measured under the same conditions. The critical micelle concentration (CMC) was calculated from the intersection of two linear fitting lines applied separately to the nearly constant region and the sharply changing region of the surface tension data.

2.6 Hydrodynamic Diameter and Zeta Potential Measurement of IPSAM

The hydrodynamic diameter of IPSAM(a/b) was determined by dynamic light scattering using an ELSZ-2000 particle size and zeta potential analyzer (Otsuka Electronics, ERAETECH, South Korea). For the measurements, IPSAM dispersions prepared at 10 mg/mL in 30 mM Trizma buffer at pH 7.0 were first diluted until the scattering intensity reached an appropriate range of 50 to 200 kcps. An aliquot of 1.5 mL was then placed in a disposable cuvette with a 2 mL capacity, and the particle size was recorded. To evaluate salt-induced changes in particle size, NaCl or $CaCl_2$ was added to the diluted IPSAM(a/b) samples to obtain final salt concentrations of 0, 20, 30, 50, 100, and 150 mM. Each sample was adjusted to a final volume of 1.5 mL, transferred into the cuvette, and analyzed under the same measurement conditions. Zeta potential was measured using the same instrument following the identical sample preparation procedure.

2.7 TEM of IPSAM(a/b)

The morphology of IPSAM was examined by transmission electron microscopy. For negative staining, a 2% phosphotungstic acid solution was prepared in distilled water and mixed for 30 min using a roller mixer. IPSAM(a/b) dispersions, prepared at 10 mg/mL in 30 mM Trizma buffer at pH 7.0, were combined with the staining solution at an equal volume ratio, giving a final phosphotungstic acid concentration of 1%. The stained dispersions were kept at room temperature in the dark for 2 h before grid preparation. Following staining, one drop of each sample was deposited

onto a copper grid and allowed to stand for 2 min. Residual liquid was gently blotted away with filter paper, after which the grid was rinsed with Trizma buffer for 1 min. The washing solution was then removed, and the grids were dried at room temperature in the dark for 24 h. Micrographs were obtained using a transmission electron microscope (LEO912AB OMEGA, LEO, Oberkochen, Germany) at the Korea Basic Science Institute. The acquired images were further processed and analyzed with Image-Pro Plus software version 5.1 from MediaCybernetics (Rockville, MD, USA).

2.8 Release Measurement of IPSAM

The release behavior of IPSAM(3/7) was investigated using Nile Red as a fluorescent probe. For dye loading, 10 µL of Nile Red stock solution at 1 mg/mL in methanol was added to 10 mL of IPSAM(3/7) dispersion prepared at 10 mg/mL in 30 mM Trizma buffer at pH 7.0 in a 20 mL vial. The mixture was then gently rolled in the dark for 24 h to allow sufficient incorporation of the fluorescent dye. For the release experiment, 2 mL of the Nile Red-loaded IPSAM(3/7) dispersion was transferred to a 3 mL cuvette. NaCl or $CaCl_2$ was then added, and 20 mM was selected as the representative salt concentration for the release test. Fluorescence intensity was monitored over time using a fluorescence spectrophotometer (Hitachi F2500, Hitachi, Japan) with an excitation wavelength of 556 nm and an emission wavelength of 613 nm. Release measurements were performed at 20, 30, 40, and 50 °C using a temperature-controlled water circulator. The release (%) of Nile Red was calculated according to Eqn. 1.

$$\text{Release}\ (\%) = (1 - \text{Ft}/\text{F0}) \times 100 \tag{1}$$

where F0 is the fluorescence intensity at time zero and Ft is the fluorescence intensity at a given time.

2.9 Nonlinear Kinetic Fitting of IPSAM Release Profiles

To quantitatively compare the release behavior of IPSAM under different temperature and salt conditions, nonlinear kinetic fitting was performed on the time-dependent Nile Red release profiles. The release percentage measured under each condition was expressed as a function of time, and the experimental data were compared with the fitted curves using Python. Data processing and calculation were performed using NumPy and pandas. Nonlinear curve fitting was conducted using the curve_fit function in SciPy, and the graphs were generated using Matplotlib. The release profiles of Nile Red were fitted according to Eqn. 2.

$$y = A\left[1 - e^{-\left(\frac{x}{\tau}\right)^{\beta}}\right] + cx \tag{2}$$

where x is the release time and y is the release percentage of Nile Red. A is the coefficient corresponding to the main release amount, τ is the coefficient representing the time scale of release, β is the coefficient representing the shape of the release curve, and c is the coefficient corresponding to the slope of the slow additional release in the later stage. The fitted curves obtained under each condition were compared with the experimental release profiles, and the goodness of fit was evaluated using R^2 and root mean square error (RMSE).

3. Results

3.1 Determination of Upper Critical Solution Temperature (UCST)

Fig. 1A shows the temperature-dependent transmittance behavior of IPSAM(a/b). The UCST values of IPSAM(3/7), IPSAM(4/6), and IPSAM(5/5) were 38.37, 33.20, and 33.38 °C, respectively, whereas those of IPSAM(6/4) and IPSAM(7/3) were below 20 °C. Among the tested formulations, IPSAM(3/7) showed the highest UCST, while IPSAM(6/4) and IPSAM(7/3) did not exhibit a phase transition within the measured temperature range. Because the UCST of IPSAM(3/7) was closest to physiological temperature, this formulation was selected for subsequent experiments. Salt concentrations ranging from 0 to 150 mM were selected by considering both physiological relevance and the need to compare ion-dependent responses. For NaCl, this range covers Na^+ concentrations reported in skin-related and body fluid environments, including human sweat, simulated wound fluid, and normal serum [22,23,24]. In contrast, the 0–150 mM $CaCl_2$ range was not intended to directly reproduce physiological Ca^{2+} concentrations, because ionized Ca^{2+} in body fluids is generally present at low millimolar levels [2,25]. Instead, $CaCl_2$ was tested over the same nominal concentration range as NaCl to compare how monovalent Na^+ and divalent Ca^{2+} differently affect the salt-responsive stability and phase transition behavior of PEI/PTA IPSAM under controlled added-salt conditions. Fig. 1B shows the temperature-dependent transmittance behavior of IPSAM(3/7) in the presence of NaCl. When NaCl was added at concentrations of 0, 20, 30, 50, 100, and 150 mM, the UCST values at 0, 20, and 30 mM were 38.37, 30.29, and 27.33 °C, respectively. At concentrations of 50 mM and above, the UCST was below 20 °C. Thus, the UCST decreased progressively as the NaCl concentration increased, and the phase transition was no longer observed within the measured temperature range at 50 mM or higher. Fig. 1C shows the temperature-dependent transmittance behavior of IPSAM(3/7) in the presence of $CaCl_2$. When $CaCl_2$ was added at concentrations of 0, 20, 30, 50, 100, and 150 mM, the UCST values at 0 and 20 mM were 38.37 and 21.02 °C, respectively, and the UCST values at 30 mM and above were below 20 °C. Overall, $CaCl_2$ caused a more pronounced reduction in UCST than NaCl at the same concentration, and the phase transition disappeared at a lower concentration in the presence of $CaCl_2$.

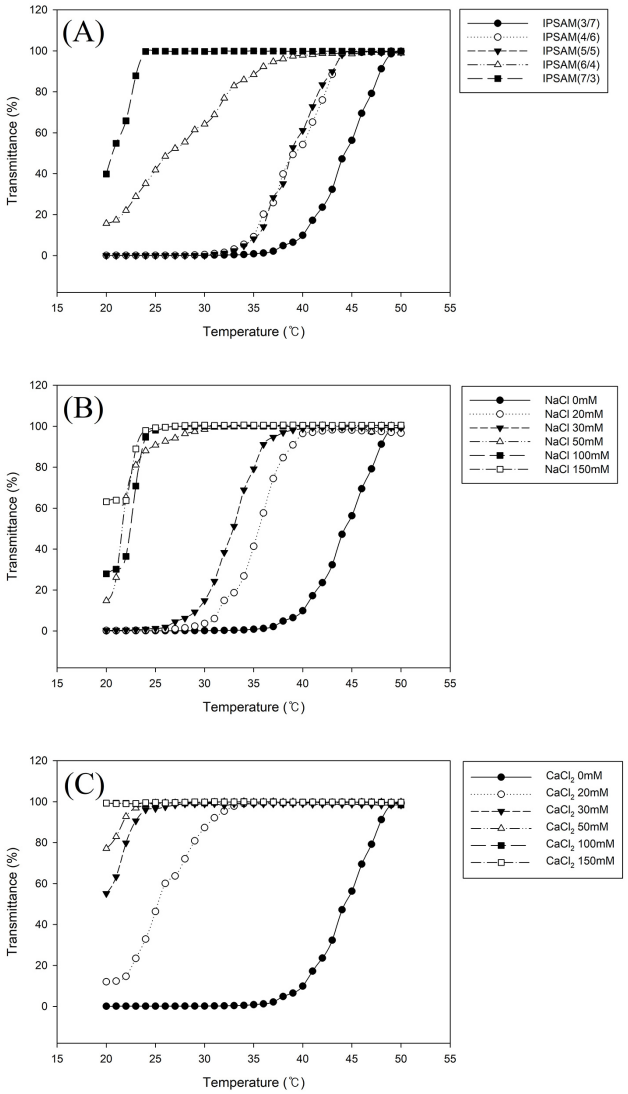

Fig. 1. Temperature-dependent transmittance profiles of PEI/PTA IPSAM suspensions under different compositional and salt conditions. (A) Transmittance profiles of IPSAM(a/b) prepared at different amino-to-carboxyl molar ratios. (B) Transmittance profiles of IPSAM(3/7) in the presence of NaCl at different concentrations. (C) Transmittance profiles of IPSAM(3/7) in the presence of $CaCl_2$ at different concentrations.

3.2 Effect of NaCl and $CaCl_2$ on the Colloidal Stability of IPSAM

Supplementary Fig. 1A shows the visual appearance of IPSAM(3/7) in the presence of NaCl. At 0 mM NaCl, the IPSAM dispersion appeared as a turbid white solution. As the NaCl concentration increased to 20, 30, 50, 100, and 150 mM, the solution gradually became more transparent. The change in appearance became more pronounced with increasing NaCl concentration, indicating a concentration-dependent change in the dispersion state of IPSAM(3/7). **Supplementary Fig. 1B** shows the visual appearance of IPSAM(3/7) in the presence of $CaCl_2$. At 0 mM $CaCl_2$, the IPSAM dispersion also appeared turbid and white. As the $CaCl_2$ concentration increased to 20, 30, 50, 100, and 150 mM, the solution progressively became more transparent. Overall, both salt conditions showed a similar concentration-dependent transition from a turbid dispersion to a clearer solution.

3.3 Results of FT-IR Analysis

Fig. 2A shows the FT-IR spectra of PEI, PTA, and IPSAM(3/7). In PEI, the band near 3288 cm^{-1}, assigned to N–H stretching, was observed. In IPSAM(3/7), this band shifted to around 3183 cm^{-1}. In PTA, the band at 1701.19 cm^{-1}, corresponding to the C=O stretching vibration of non-ionized carboxylic acid, was observed. However, in IPSAM(3/7), the band near 1701 cm^{-1} became relatively weaker, while distinct carboxylate-related bands appeared at 1629.55 cm^{-1} and 1551.78 cm^{-1}. Fig. 2B shows the FT-IR spectra of IPSAM(3/7) in the presence of NaCl. NaCl concentrations of 20 mM and 150 mM were selected as representative low and high concentrations, respectively. After NaCl addition, the NH_3^+-related band near 3183 cm^{-1} became weaker, while a stretching band reappeared near 3325 cm^{-1}. In the COO^- region, the bands originally separated at approximately 1629 cm^{-1} and 1552 cm^{-1} became weaker or less clearly resolved after salt addition. In particular, under the 150 mM condition, these bands tended to converge into a broad single band near 1629 cm^{-1}. Fig. 2C shows the FT-IR spectra of IPSAM(3/7) in the presence of $CaCl_2$. $CaCl_2$ concentrations of 20 mM and 150 mM were selected as representative conditions. After $CaCl_2$ addition, the NH_3^+-related band near 3183 cm^{-1} also decreased, while the intensity of the stretching band near 3355 cm^{-1} increased. In addition, the intensity of the carboxylate-related band near 1581 cm^{-1} decreased, whereas the carboxylic acid C=O band near 1703 cm^{-1} became more pronounced.

3.4 Results of Surface Tension Measurement

Fig. 3A shows the surface tension of PEI, PTA, and IPSAM(a/b). At 20 mg/mL, the surface tension values of IPSAM(3/7), IPSAM(4/6), IPSAM(5/5), IPSAM(6/4), and IPSAM(7/3) were 48.0370, 48.1128, 48.6458, 48.4967, and 48.7569 dyne/cm, respectively. In contrast, the surface tension values of PEI and PTA alone were 72.6560 and 51.4096 dyne/cm, respectively. Upon two-fold serial dilution, the IPSAM samples exhibited a typical L-shaped profile. Fig. 3B shows the change in surface tension of IPSAM(3/7) in the presence of NaCl. At 20 mg/mL, the surface tension values at NaCl concentrations of 0, 20, 30, 50, 100, and 150 mM were 48.5723, 50.0135, 50.3514, 50.1884, 49.5563, and 50.1212 dyne/cm, respectively. Overall, the surface tension increased after NaCl addition. Fig. 3C shows the change in surface tension of IPSAM(3/7) in the presence of $CaCl_2$. At 20 mg/mL, the surface tension values at $CaCl_2$ concentrations of 0, 20, 30, 50, 100, and 150 mM were 48.5723, 48.7123, 49.4759, 49.7656, 49.4637, and 49.2369 dyne/cm, respectively. A

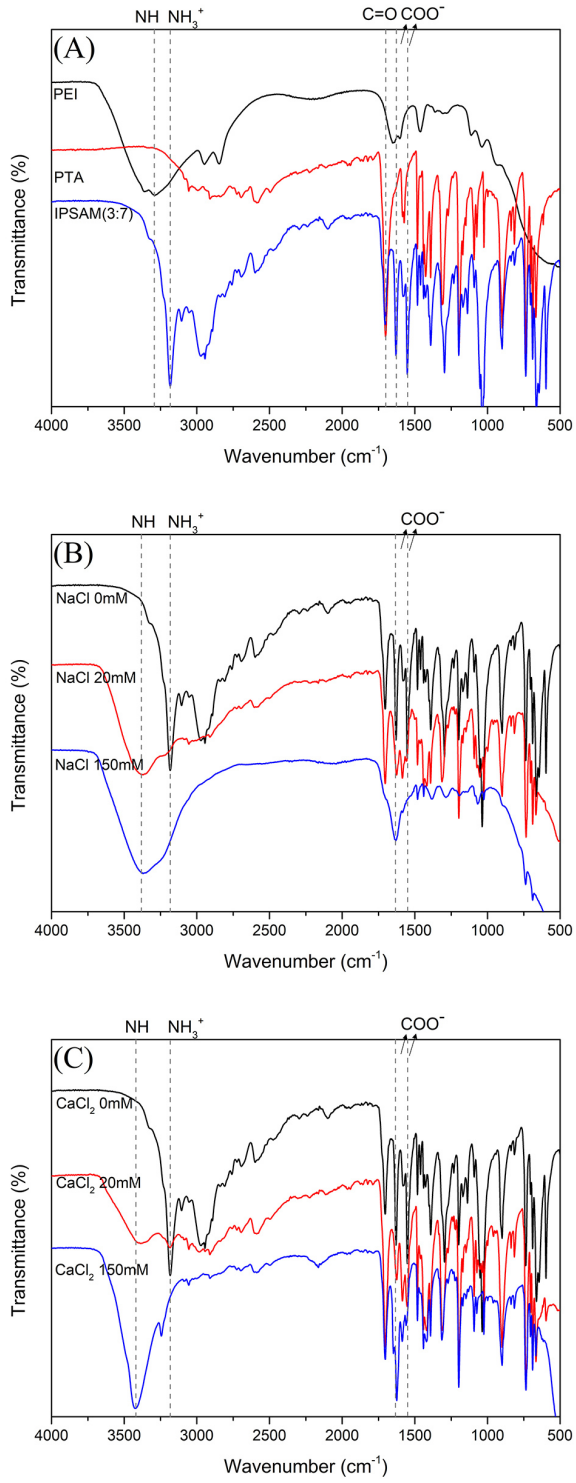

Fig. 2. FT-IR spectra of PEI, PTA, and IPSAM(3/7) under different salt conditions. (A) FT-IR spectra of PEI, PTA, and IPSAM(3/7). (B) FT-IR spectra of IPSAM(3/7) in the presence of NaCl at 0, 20, and 150 mM. (C) FT-IR spectra of IPSAM(3/7) in the presence of $CaCl_2$ at 0, 20, and 150 mM. FT-IR, fourier-transform infrared.

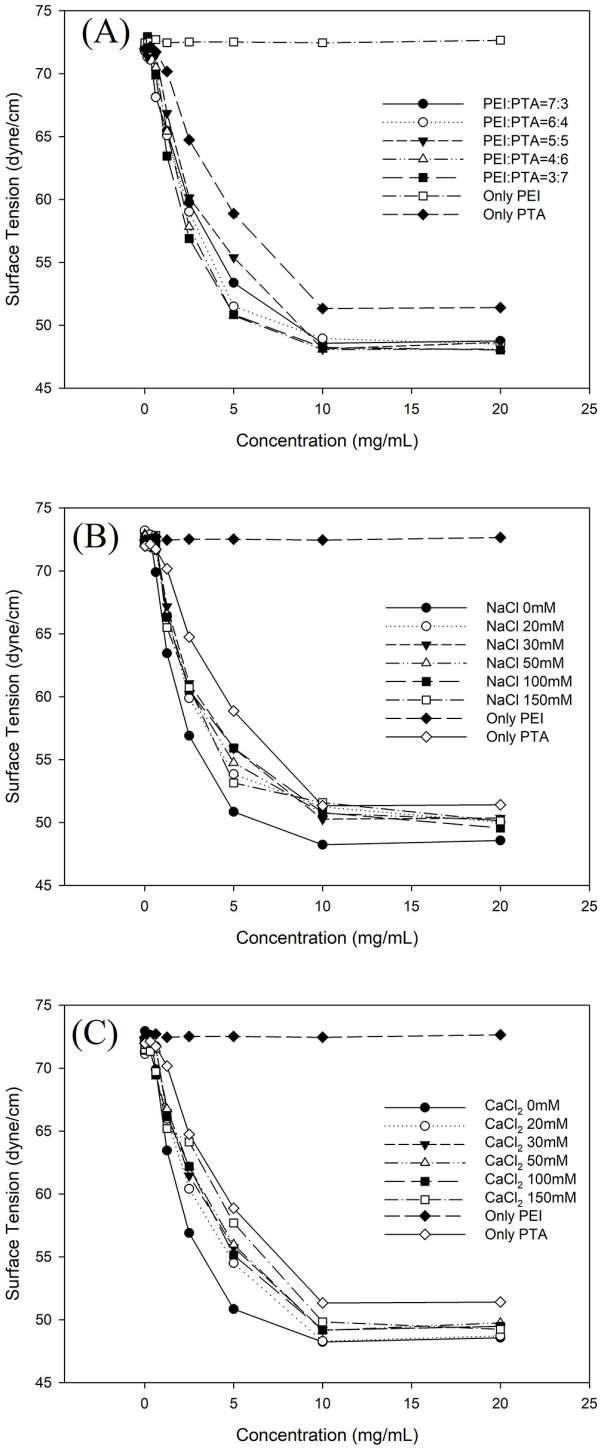

Fig. 3. Surface tension profiles of PEI, PTA, and IPSAM under different salt conditions. (A) Surface tension profiles of PEI, PTA, and IPSAM(a/b). (B) Surface tension profiles of IPSAM(3/7) in the presence of NaCl at different concentrations. (C) Surface tension profiles of IPSAM(3/7) in the presence of $CaCl_2$ at different concentrations.

similar increasing trend in surface tension was also observed after $CaCl_2$ addition. To further evaluate the effect of salt on micelle formation, the CMC of IPSAM(3/7) was calculated from the surface tension profiles. The CMC of IPSAM(3/7) without salt was 8.08 mg/mL. After NaCl treat-

ment at 20, 30, 50, 100, and 150 mM, the CMC values were 9.14, 9.99, 9.39, 10.46, and 8.74 mg/mL, respectively. In all NaCl treatment samples, the CMC values were higher than that of untreated IPSAM(3/7). Similarly, after $CaCl_2$ treatment at 20, 30, 50, 100, and 150 mM, the CMC values were 10.01, 10.57, 10.73, 11.12, and 14.05 mg/mL, respectively. These results show that $CaCl_2$ treatment increased the CMC more markedly than NaCl treatment.

3.5 Results of Hydrodynamic Diameter and Zeta Potential Measurement

Fig. 4A shows the changes in particle size and zeta potential of IPSAM(3/7) in the presence of NaCl. At NaCl concentrations of 0, 20, 30, 50, 100, and 150 mM, the particle sizes were 265.3, 417.7, 567.3, 3020.9, 2950.4, and 3064.7 nm, respectively, showing an overall increasing trend with increasing NaCl concentration. In contrast, the zeta potential values were 59.08, 49.98, 47.91, 44.32, 31.12, and 23.43 mV, respectively, showing a decreasing trend as the NaCl concentration increased. In particular, the particle size increased sharply at 50 mM and remained at a similar level at higher concentrations. Fig. 4B shows the changes in particle size and zeta potential of IPSAM(3/7) in the presence of $CaCl_2$. At $CaCl_2$ concentrations of 0, 20, 30, 50, 100, and 150 mM, the particle sizes were 265.3, 2025.9, 2451.8, 2829.2, 3148.9, and 3357.7 nm, respectively, while the zeta potential values were 59.08, 50.05, 49.51, 39.72, 17.20, and 1.15 mV, respectively. Similar increases in particle size and decreases in zeta potential were observed in the presence of $CaCl_2$. Compared with NaCl, these changes were more pronounced at lower concentrations in the presence of $CaCl_2$.

3.6 TEM Imaging and Image Analysis

Fig. 5A shows the transmission electron microscopy (TEM) image of IPSAM in the absence of added salt. Spherical nanoparticles were observed, and the particles displayed a relatively dark outer region and a brighter interior. Under this condition, the particle boundaries were relatively clear, allowing the morphology of individual particles to be distinguished. Fig. 5B shows the TEM image of IPSAM in the presence of NaCl. To clearly observe salt-induced structural changes, the sample was examined at the highest NaCl concentration. Compared with the sample without added salt, the salt-treated sample showed a loss of morphological integrity, as evidenced by poorly defined particle boundaries and reduced particle contrast. Fig. 5C shows the TEM image of IPSAM in the presence of $CaCl_2$. The sample was also examined at the highest $CaCl_2$ concentration. Similar to the NaCl-treated sample, $CaCl_2$-treated IPSAM showed a marked loss of morphological integrity and structural dissociation. The particle boundaries became poorly defined, and individual particles were difficult to distinguish. These observations suggest that both NaCl and $CaCl_2$ disrupted the micellar structure of IPSAM, leading to a less organized morphology consistent with random-coil-like structures.

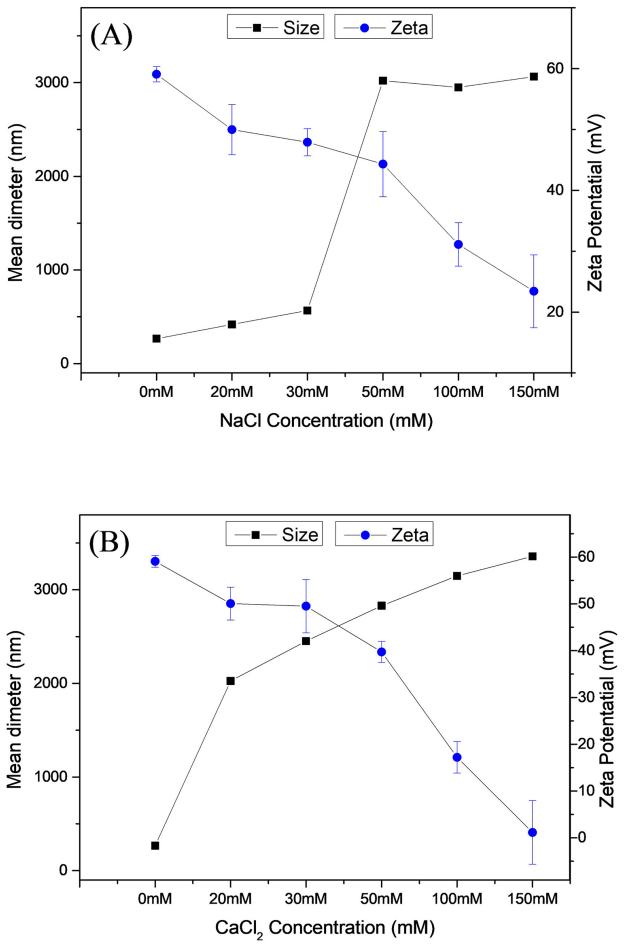

Fig. 4. Hydrodynamic diameter and zeta potential of IPSAM(3/7) under different salt conditions. (A) Hydrodynamic diameter and zeta potential of IPSAM(3/7) in the presence of NaCl at different concentrations. (B) Hydrodynamic diameter and zeta potential of IPSAM(3/7) in the presence of $CaCl_2$ at different concentrations.

3.7 Release Measurement

Fig. 6A shows the temperature-dependent release behavior of IPSAM(3/7) in the absence of added salt. The release percentages at 20, 30, 40, and 50 °C were 4.25, 10.83, 25.98, and 41.38%, respectively, showing that the release increased with increasing temperature. Release experiments in the presence of NaCl and $CaCl_2$ were performed at salt concentration of 20 mM because IPSAM(3/7) still showed measurable UCST values in the presence of both salts within the experimental temperature range (Fig. 1B,C). At higher concentrations, the dispersions became transparent, suggesting that the self-assembled structures were already destabilized (**Supplementary Fig. 1A**,**B**). Therefore, 20 mM was chosen as the representative condition for comparing temperature-dependent release under

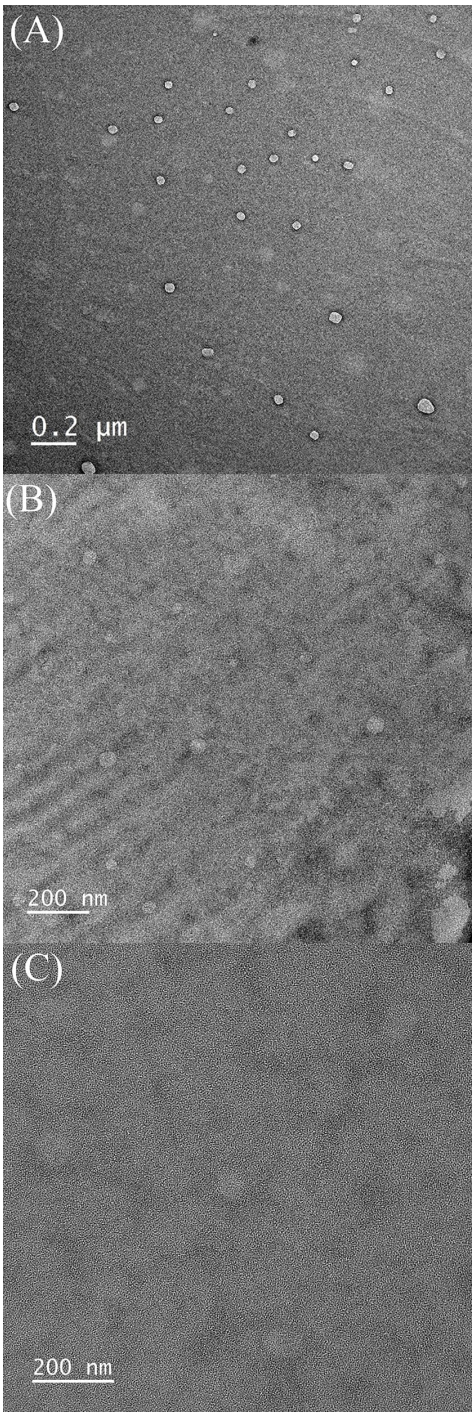

Fig. 5. TEM images of IPSAM(3/7) under different salt conditions. (A) TEM image of IPSAM(3/7) in the absence of added salt. (B) TEM image of IPSAM(3/7) in the presence of NaCl. (C) TEM image of IPSAM(3/7) in the presence of $CaCl_2$. TEM, transmission electron microscopy. The scale bar in (A–C) represents 200 nm.

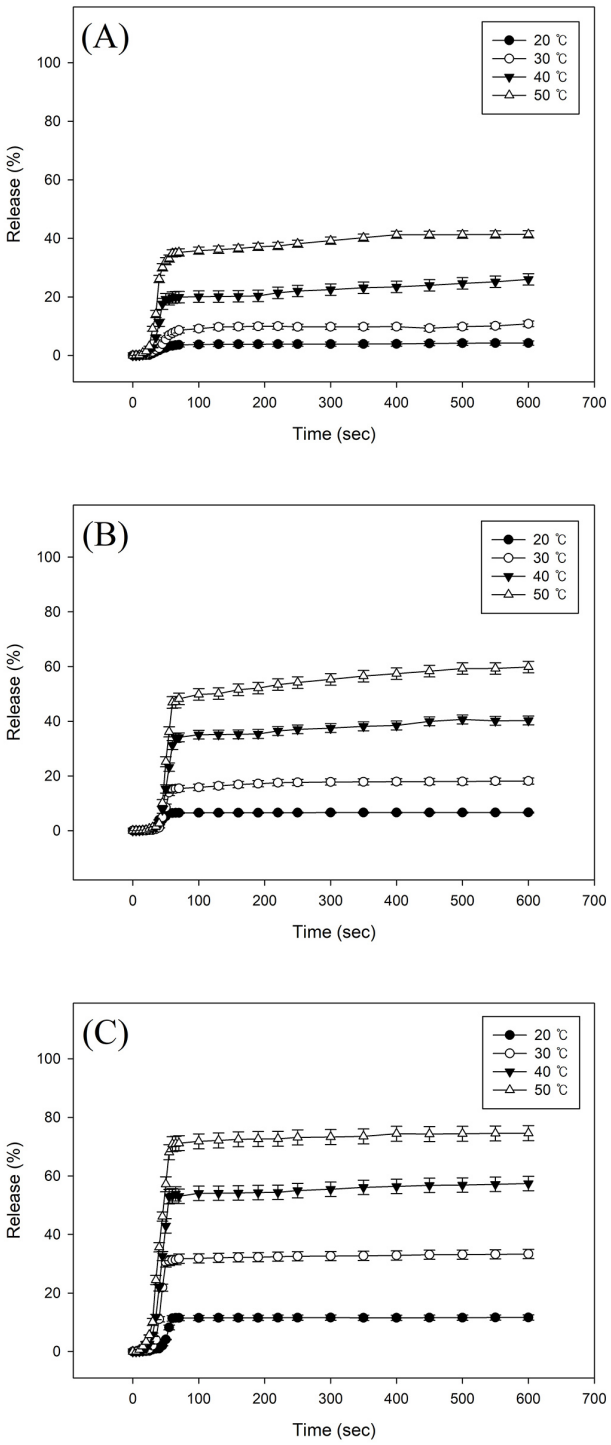

Fig. 6. Release profiles of IPSAM(3/7) under different temperature and salt conditions. (A) Release profiles of IPSAM(3/7) at different temperatures in the absence of added salt. (B) Release profiles of IPSAM(3/7) at different temperatures in the presence of NaCl. (C) Release profiles of IPSAM(3/7) at different temperatures in the presence of $CaCl_2$.

both salt conditions. Fig. 6B shows the temperature-dependent release behavior of IPSAM(3/7) in the presence of 20 mM NaCl. The release percentages at 20, 30, 40, and 50 °C were 6.64, 18.14, 40.27, and 59.85%, respectively. These values were generally higher than those observed under salt-free conditions. Fig. 6C shows the temperature-dependent release behavior of IPSAM(3/7) in the presence

Table 1. Weibull-type nonlinear fitting equations and goodness-of-fit parameters for Nile Red release from IPSAM(3/7) under different temperature and salt conditions.

Salt condition	Temperature (°C)	Fitting equation	R^2	RMSE
No salt	20	$y = 3.6042\left[1 - e^{-(\frac{x}{45.8654})^{3.6832}}\right] + 0.001088x$	0.9976	0.0793
	30	$y = 9.3909\left[1 - e^{-(\frac{x}{52.8973})^{3.6462}}\right] + 0.001355x$	0.9956	0.2707
	40	$y = 18.8467\left[1 - e^{-(\frac{x}{40.5189})^{6.9592}}\right] + 0.011611x$	0.9989	0.3027
	50	$y = 33.9945\left[1 - e^{-(\frac{x}{38.7825})^{5.0851}}\right] + 0.014878x$	0.9970	0.8575
NaCl	20	$y = 6.4958\left[1 - e^{-(\frac{x}{44.0141})^{4.8630}}\right] + 0.000261x$	0.9941	0.2121
	30	$y = 15.7008\left[1 - e^{-(\frac{x}{51.3062})^{9.2882}}\right] + 0.005011x$	0.9972	0.4156
	40	$y = 33.4817\left[1 - e^{-(\frac{x}{53.9630})^{8.1929}}\right] + 0.012765x$	0.9993	0.4321
	50	$y = 47.4156\left[1 - e^{-(\frac{x}{52.8077})^{9.0993}}\right] + 0.023290x$	0.9986	0.9369
$CaCl_2$	20	$y = 11.5283\left[1 - e^{-(\frac{x}{53.7329})^{9.6984}}\right] + 0.000182x$	0.9979	0.2413
	30	$y = 31.3804\left[1 - e^{-(\frac{x}{44.0817})^{8.6078}}\right] + 0.003675x$	0.9996	0.2951
	40	$y = 53.3153\left[1 - e^{-(\frac{x}{45.3313})^{5.4578}}\right] + 0.007141x$	0.9995	0.5475
	50	$y = 71.5160\left[1 - e^{-(\frac{x}{44.1900})^{4.2745}}\right] + 0.005815x$	0.9990	0.9245

The release profiles were fitted using Weibull-type nonlinear equations, and the fitting quality was evaluated using R^2 and RMSE. RMSE, root mean square error.

of 20 mM $CaCl_2$. The release percentages at 20, 30, 40, and 50 °C were 11.63, 33.34, 57.41, and 74.61%, respectively. Under the $CaCl_2$ condition, the release percentage also increased markedly with increasing temperature, and higher release was observed across the entire temperature range than under both salt-free and NaCl conditions.

3.8 Results of Nonlinear Kinetic Fitting

Table 1 shows the Weibull-type nonlinear fitting equations and goodness-of-fit parameters obtained under different temperature and salt conditions. R^2 indicates how well the fitting equation explains the experimental release profile, whereas RMSE represents the average error between the experimental values and the fitting curve. The R^2 values were higher than 0.9941 under all conditions, indicating that the applied fitting equations adequately described the time-dependent Nile Red release profiles. In addition, the RMSE values were close to zero, confirming that the differences between the experimental values and the fitting curves were small. As shown in **Supplementary Fig. 2**, the dots represent the experimental data, while the solid lines represent the fitting curves obtained from the fitting equations. The experimental data and fitting curves showed overall similar release profiles, supporting the high R^2 and low RMSE values shown in Table 1. To compare the effects of temperature and salt conditions on the release behavior, the A coefficient in the fitting equation was mainly analyzed. Since the A coefficient corresponds to the main release amount, it is suitable for comparing changes in release amount under different conditions. In the absence of added salt, the A value increased with increasing temperature from 3.6042 at 20 °C to 9.3909 at 30 °C, 18.8467 at 40 °C, and 33.9945 at 50 °C. Under the NaCl condition, the A value also increased from 6.4958 at 20 °C to 15.7008 at 30 °C, 33.4817 at 40 °C, and 47.4156 at 50 °C. Under the $CaCl_2$ condition, the A value increased from 11.5283 at 20 °C to 31.3804 at 30 °C, 53.3153 at 40 °C, and 71.5160 at 50 °C. The $CaCl_2$ condition showed the highest A value among the three conditions at all temperatures.

4. Discussion

4.1 Interpretation of UCST Results

These results indicate that the phase transition behavior of IPSAM was affected by both the PEI and PTA composition and the type and concentration of added salt. The higher UCST observed in formulations containing a larger proportion of PTA suggests that hydrophobic interactions within IPSAM became stronger as the PTA content increased. In other words, a higher content of the hydrophobic PTA component likely required greater thermal energy to dissociate the self-assembled IPSAM structure, thereby leading to an increase in UCST. In the presence of NaCl or $CaCl_2$, the UCST decreased markedly, indicating that dissolved ions weakened the electrostatic ion pair interactions responsible for maintaining the stability of IPSAM. This effect can be attributed to electrostatic screening by salt ions, which reduced the direct attractive force between the protonated amino groups of PEI and the carboxylate groups of PTA. In addition, externally added ions

likely interacted competitively with these charged groups, thereby disturbing the ionic environment that stabilized the ion paired structure. For $CaCl_2$, this effect can become more pronounced because divalent Ca^{2+} provides stronger charge screening than monovalent Na^+, thereby more effectively perturbing the electrostatic interactions between the protonated amino groups of PEI and the carboxylate groups of PTA [26,27,28]. In addition, previous studies have reported that Ca^{2+} can interact with carboxylate-containing polyelectrolytes through binding or bridging interactions [29,30]. Therefore, in PEI/PTA IPSAM, Ca^{2+} may also interact with the carboxylate groups of PTA, which could partly contribute to the greater decrease in UCST observed after $CaCl_2$ treatment than after NaCl treatment.

4.2 Interpretation of Colloidal Stability Under NaCl and $CaCl_2$ Conditions

The turbid white appearance observed in the absence of added salt suggests the successful formation of IPSAM particles. This is because the amino groups of PEI and the carboxyl groups of PTA formed ion pairs through electrostatic attraction, and these ion pairs subsequently self-assembled in aqueous solution to generate colloidal particles. In general, colloidal particles scatter visible light, and thus a white or turbid appearance suggests the successful formation of IPSAM [31,32,33]. In contrast, as the concentrations of NaCl and $CaCl_2$ increased, the solutions gradually became more transparent. This change is likely due to the interference of salt-derived ions with the electrostatic ion pair interactions within IPSAM, resulting in reduced colloidal stability. As the salt concentration increased, a greater number of ions interacted with the ion paired structure formed between PEI and PTA, thereby weakening the electrostatic interactions. As a result, the self-assembled colloidal structure gradually collapsed and the particles could no longer remain stably dispersed. Consequently, the colloidal structures responsible for scattering visible light were reduced or lost, leading to a more transparent appearance of the solution.

4.3 Interpretation of FT-IR Results

The shift of the N–H stretching band from 3288 cm^{-1} in PEI to around 3183 cm^{-1} in IPSAM(3/7) suggests the formation of an NH_3^+ environment due to protonation of the amine groups. In addition, the weakening of the C=O stretching band of non-ionized carboxylic acid near 1701 cm^{-1} and the appearance of distinct carboxylate-related bands at 1629.55 cm^{-1} and 1551.78 cm^{-1} indicate an increase in the COO^- form following deprotonation of the carboxylic acid groups. These changes support the formation of ion pairs between the protonated amine groups of PEI and the carboxylate groups of PTA. After the addition of NaCl or $CaCl_2$, the NH_3^+-related band near 3183 cm^{-1} became weaker, and changes were also observed in the carboxylate-related region. Under these conditions, the reappearance or increase of bands associated with N–H stretching or carboxylic acid C=O stretching, together with the weakening or merging of carboxylate-related bands, suggests that salt addition altered the ion pair interaction environment in IPSAM. This change may be attributed to electrostatic screening and competitive interactions of externally added ions with the charged groups of PEI and PTA, which could weaken or rearrange the ion paired structure. These spectral changes indicate that added salts modified the local bonding environment surrounding the protonated amine groups and carboxylate groups within IPSAM.

4.4 Interpretation of Surface Tension Results

The L-shaped surface tension profile observed for the IPSAM samples is characteristic of amphiphilic materials that adsorb at the interface and then show a smaller change in surface tension above a certain concentration [34,35,36]. This result suggests that the hydrophilic cationic polymer PEI and the hydrophobic counterion PTA formed ion pairs through electrostatic attraction, thereby generating an amphiphilic structure. In addition, the lower surface tension of IPSAM compared with PTA alone indicates that ion pair formation enhanced the interfacial activity and enabled more effective arrangement at the interface, thereby reducing the surface free energy. After the addition of NaCl or $CaCl_2$, the surface tension of IPSAM(3/7) increased overall. These changes suggest that added salt ions altered the ionic interaction environment between PEI and PTA and affected the interfacial adsorption behavior of the ion pair self-assembled structure. This effect may be attributed to electrostatic screening or competitive interactions of externally added ions with the charged groups of PEI and PTA, which could weaken or rearrange the ion pair interactions. As a result, the interfacial organization of IPSAM may have become less favorable for reducing surface tension. In addition, the CMC was calculated from the intersection of two linear regions in the surface tension profile: the concentration-dependent decreasing region and the high-concentration plateau region. In conventional amphiphilic assemblies, added salts can enhance hydrophobic interactions between nonpolar segments through a salting-out effect and stabilize the assembled structure, often leading to a decrease in CMC [37,38]. However, IPSAM showed the opposite behavior. Although hydrophobic interactions may be strengthened in the presence of salt, the amphiphilic structure of IPSAM is maintained by PEI/PTA ion pair interactions. External ions can compete with and disrupt these ion pairs, thereby weakening the effective amphiphilicity. As a result, a higher concentration is required for micelle formation, leading to an increase in CMC. The more pronounced increase in CMC after $CaCl_2$ treatment suggests that divalent Ca^{2+} more effectively interfered with the ion pair structure than monovalent Na^+, consistent with its stronger interaction with carboxylate groups.

4.5 Interpretation of Hydrodynamic Diameter and Zeta Potential Measurement Results

These results suggest that added salts altered the colloidal stability of IPSAM(3/7). In the presence of NaCl, the increase in particle size together with the decrease in zeta potential suggests that salt ions screened the surface charges of IPSAM, thereby reducing the electrostatic repulsion between particles and promoting aggregation [39,40,41]. The sharp increase in particle size at 50 mM and the similar values observed above this concentration further suggest that aggregation had already progressed substantially at and above this salt concentration. A similar trend was observed in the presence of $CaCl_2$, but the changes were more pronounced at lower concentrations than in the presence of NaCl. This difference may be attributed to the divalent Ca^{2+} ions, which can screen the surface charges of IPSAM more effectively than monovalent Na^+ ions, thereby more strongly reducing the electrostatic repulsion between particles. In addition, previous studies have reported that Ca^{2+} can interact with carboxylate-containing polyelectrolytes through binding or bridging interactions [29,30]. Therefore, Ca^{2+} may also interact with the carboxylate groups of PTA in PEI/PTA IPSAM, which could partly contribute to the more pronounced changes in particle size and zeta potential observed after $CaCl_2$ treatment. In PEI/PTA IPSAM, such Ca^{2+}–carboxylate interactions could alter the local ionic environment of the PTA carboxylate groups and partially reorganize the original PEI–PTA ion pair, thereby promoting aggregation more effectively than Na^+. As a result, $CaCl_2$ appears to destabilize the IPSAM dispersion more effectively than NaCl.

4.6 Interpretation of TEM Results

The relatively dark outer region and brighter interior observed in the sample without added salt may be attributed to the electron density contrast generated during the negative staining process [42,43]. Under this condition, the particles exhibited relatively clear boundaries and distinguishable spherical morphology, suggesting that IPSAM maintained its original self-assembled organization in the absence of added salt. In contrast, after the addition of NaCl or $CaCl_2$, the particle contrast and boundaries became less distinct, and the morphology of individual particles were no longer clearly resolved. These changes suggest that added salt ions affected the original organization or dispersion state of IPSAM. Taken together with the UCST, FT-IR, particle size, and zeta potential results, these observations further support that added salts perturbed the ionic interactions responsible for stabilizing IPSAM. Such perturbation likely reduced the morphological integrity of the particles and altered their dispersion behavior. Consequently, the added salts appear to have reduced the structural uniformity and colloidal stability of IPSAM, which was reflected by the less distinct TEM images.

4.7 Interpretation of Release Results

The temperature-dependent release behavior of IPSAM(3/7) can be interpreted in relation to its UCST-based phase transition. As shown in Fig. 1A, IPSAM(3/7) exhibited a UCST of 38.37 °C, indicating that the ion pair self-assembled structure remained relatively stable below this temperature but became more easily loosened or rearranged as the temperature approached or exceeded the transition point. This interpretation is consistent with the increase in release at higher temperatures. In the presence of NaCl or $CaCl_2$, the release was further enhanced because the added ions had already perturbed the ionic interactions responsible for maintaining the IPSAM structure before thermal activation. Taken together, these results indicate that added salts weakened or rearranged the ion pair interaction of IPSAM, allowing the structure to be destabilized more readily and facilitating release even under the same thermal conditions. Under these salt-containing conditions, most of the fluorescence signal increased rapidly within the initial 60 s and then reached a plateau-like equilibrium state. This suggests that salt-induced perturbation of the PEI/PTA ion pair interactions promoted rapid Nile Red release at the early stage, rather than sustained time-dependent release over a prolonged period. The higher release observed in the presence of $CaCl_2$ than in the presence of NaCl is also consistent with the above results showing that $CaCl_2$ caused a greater reduction in UCST and more pronounced changes in particle size and zeta potential. This stronger effect can be associated with the divalent nature of Ca^{2+}. Compared with monovalent Na^+, Ca^{2+} can provide stronger charge screening and more effectively perturb the ionic interaction network of PEI/PTA IPSAM [26,27,28]. In addition, previous studies have reported that Ca^{2+} can interact with carboxylate-containing polyelectrolytes through binding or bridging interactions [29,30]. Therefore, in PEI/PTA IPSAM, Ca^{2+} may also interact with the carboxylate groups of PTA, which could partly contribute to the higher Nile Red release observed under $CaCl_2$ conditions than under NaCl conditions. To further evaluate whether salt treatment and temperature elevation produced an additive or enhanced combined effect, the release data were reanalyzed using an additive rule. The release at 20 °C without added salt was used as the baseline. The expected additive release was calculated by adding the temperature-induced release increase under salt-free conditions and the salt-induced release increase at 20 °C to this baseline value. For NaCl, the expected additive releases at 30, 40, and 50 °C were 13.22, 28.37, and 43.77%, respectively, whereas the observed releases were 18.14, 40.27, and 59.85%, respectively. These observed values were higher than the expected additive values, indicating that NaCl and temperature elevation enhanced Nile Red release beyond a simple additive response. For $CaCl_2$, the expected additive releases at 30, 40, and 50 °C were 18.21, 33.36, and 48.76%, respectively, whereas the observed releases were 33.34, 57.41, and 74.61%, re-

Table 2. Summary of the effects of NaCl and $CaCl_2$ on the UCST, CMC, size, and release behavior of IPSAM.

Parameter	Salt	Salt concentration (mM)					
		0 mM	20 mM	30 mM	50 mM	100 mM	150 mM
UCST (°C)	NaCl	38.37	30.29	27.33	<20	<20	<20
	$CaCl_2$	38.37	21.02	<20	<20	<20	<20
CMC (mg/mL)	NaCl	8.08	9.14	9.99	9.39	10.46	8.74
	$CaCl_2$	8.08	10.01	10.57	10.73	11.12	14.05
Size (nm)	NaCl	265.3	417.7	567.3	3020.9	2950.4	3064.7
	$CaCl_2$	265.3	2025.9	2451.8	2829.2	3148.9	3357.7
		Temperature (°C)					
		20 °C		30 °C	40 °C	50 °C	
Release (%)	NaCl	6.64		18.14	40.27	59.85	
	$CaCl_2$	11.63		33.34	57.41	74.61	

UCST, CMC, and size were evaluated at different salt concentrations, whereas release was measured at different temperatures at a fixed salt concentration of 20 mM. Values shown as <20 °C indicate that no clear UCST transition was observed within the measured temperature range. UCST, upper critical solution temperature; CMC, critical micelle concentration.

spectively. The larger positive differences observed under $CaCl_2$ conditions indicate that $CaCl_2$ produced a stronger salt–temperature interaction than NaCl. These results suggest that salt treatment and temperature elevation did not merely act in the same direction but jointly enhanced the destabilization of PEI/PTA IPSAM and promoted Nile Red release. To provide a concise summary of all the preceding results, the effects of NaCl and $CaCl_2$ on the UCST, CMC, particle size, and release behavior of IPSAM are summarized in Table 2.

4.8 Interpretation of Nonlinear Kinetic Fitting Results

Weibull-type nonlinear fitting analysis confirmed that the Nile Red release behavior of IPSAM changed quantitatively depending on temperature and salt conditions. The high R^2 values and low RMSE values obtained under all conditions indicate that the applied fitting equation appropriately described the time-dependent release profiles. Under the salt-free condition, the A coefficient, which represents the main release amount, increased with increasing temperature. In particular, the A value increased markedly near or above the UCST of IPSAM(3/7), which was 38.37 °C. This result suggests that the IPSAM structure became loosened or rearranged above the UCST, thereby increasing the releasable fraction of Nile Red. Under the NaCl and $CaCl_2$ conditions, the A value also increased with increasing temperature and was higher than that under the salt-free condition at the same temperature. As shown in Fig. 1, the UCST values of IPSAM(3/7) decreased to 30.29 °C and 21.02 °C after the addition of 20 mM NaCl and 20 mM $CaCl_2$, respectively. Therefore, the increased A values under salt conditions can be interpreted as a result of the salt-induced decrease in UCST, which increased the releasable fraction of Nile Red even at lower temperatures. In addition, when the A values were compared at the same temperature under salt-treated conditions, the $CaCl_2$ condition always showed higher values than the NaCl condition. This quantitatively confirmed that $CaCl_2$ had a stronger effect on the release behavior of IPSAM than NaCl. Consistent with the previous results, this finding suggests that divalent Ca^{2+} reduced the ion-pair structural stability of IPSAM more strongly than monovalent Na^+, thereby facilitating Nile Red release.

4.9 Limitations

The NaCl concentration range used in this study was selected considering physiologically relevant conditions, whereas $CaCl_2$ was tested over the same concentration range as NaCl to compare the effects of monovalent and divalent ions. Therefore, the salt-responsive behavior observed in this study may differ from that in actual physiological environments containing various ions and biological components. In addition, Nile Red was used as the payload in this study, and the loading and release behavior may differ when actual therapeutic drugs are incorporated, depending on their physicochemical properties. Therefore, further *in vitro* and *in vivo* studies using therapeutic drug-loaded IPSAM are required to evaluate its practical applicability.

5. Conclusions

In this study, PEI/PTA IPSAM nanoparticles were prepared, and their responses to temperature and salt were systematically investigated. Among the tested formulations, IPSAM(3/7) exhibited a UCST of 38.37 °C, which was closest to physiological temperature and was therefore selected for further study. In the presence of NaCl and $CaCl_2$, the UCST decreased markedly, indicating that external ions weakened or rearranged the ionic interactions responsible

for maintaining the self-assembled structure. FT-IR analysis showed changes in the amine- and carboxylate-related bands after salt addition, supporting that the ionic interaction environment of IPSAM was altered in the presence of salts. Surface tension measurements showed that IPSAM possessed amphiphilic interfacial properties, while the increase in surface tension after salt addition suggested that external ions also affected the interfacial behavior of the self-assembled structure. These salt-induced changes were further supported by increased transparency, reduced zeta potential, enlarged particle size, and less distinct particle morphology in TEM images. Moreover, Nile Red release increased with increasing temperature and was further enhanced in the presence of salts, with a more pronounced effect observed in the presence of $CaCl_2$ than NaCl. Taken together, these results demonstrate that PEI/PTA IPSAM functions as a nanocarrier responsive to both temperature and salt. These findings suggest that PEI/PTA IPSAM can remain relatively stable under low-salt formulation or storage conditions, but after topical application to the skin, skin-relevant ionic and thermal conditions may destabilize the assembled structure and promote payload release. This storage-stable and application-triggered switching behavior supports the potential applicability of PEI/PTA IPSAM in topical pharmaceutical and cosmetic delivery formulations. Overall, the present findings provide useful insight into the design of ion pair nanocarriers with temperature- and salt-responsive behavior.

Availability of Data and Materials

All data obtained in this study are included in the article.

Author Contributions

Data curation, visualization, and drafting of the manuscript were performed by JSH. Material preparation, experiments, and data collection were performed by WL. Conceptualization and research direction were performed by J-CK. All authors read and approved the final manuscript. All authors contributed to editorial changes in the manuscript. All authors have participated sufficiently in the work and agreed to be accountable for all aspects of the work.

Ethics Approval and Consent to Participate

Not applicable.

Acknowledgment

We would like to express our gratitude to all those who helped us during the writing of this manuscript. Thanks to all the peer reviewers for their opinions and suggestions.

Funding

This research was supported by Basic Science Research Program through the National Research Foundation of Korea (NRF) funded by the Ministry of Education (No. RS-2018-NR031068) and this work was supported by the National Research Foundation of Korea (NRF) grant funded by the Korea government (MSIT) (No. RS-2022-NR070087).

Conflicts of Interest

The authors declare no conflicts of interest.

Declaration of AI and AI-Assisted Technologies in the Writing Process

During the preparation of this work the authors used ChatGpt-4.2 in order to check spelling and grammar. After using this tool, the authors reviewed and edited the content as needed and take full responsibility for the content of the publication.

Supplementary Material

Supplementary material associated with this article can be found, in the online version, at https://doi.org/10.31083/DJNB52488.

References

[1] Baker LB, Wolfe AS. Physiological mechanisms determining eccrine sweat composition. European Journal of Applied Physiology. 2020; 120: 719–752. https://doi.org/10.1007/s00421-020-04323-7

[2] Svensby AU, Nygren E, Gefen A, Cullen B, Ronkvist ÅM, Gergely A, et al. The importance of the simulated wound fluid composition and properties in the determination of the fluid handling performance of wound dressings. International Wound Journal. 2024; 21: e14861. https://doi.org/10.1111/iwj.14861

[3] Schwerdt G, Schulz MC, Kopf M, Mildenberger S, Reime S, Gekle M. Physiological regulation of oral saliva ion composition and flow rate are not coupled in healthy humans-Partial revision of our current knowledge required. Pflügers Archiv: European Journal of Physiology. 2025; 477: 55–65. https://doi.org/10.1007/s00424-024-03025-9

[4] Kim D, Matsuoka H, Yusa SI, Saruwatari Y. Collapse Behavior of Polyion Complex (PIC) Micelles upon Salt Addition and Reforming Behavior by Dialysis and Its Temperature Responsivity. Langmuir: the ACS Journal of Surfaces and Colloids. 2020; 36: 15485–15492. https://doi.org/10.1021/acs.langmuir.0c02456

[5] Cao T, Elimelech M. Colloidal stability of cellulose nanocrystals in aqueous solutions containing monovalent, divalent, and trivalent inorganic salts. Journal of Colloid and Interface Science. 2021; 584: 456–463. https://doi.org/10.1016/j.jcis.2020.09.117

[6] Gade L, Boyd BJ, Malmsten M, Heinz A. Stimuli-responsive drug delivery systems for inflammatory skin conditions. Acta Biomaterialia. 2024; 187: 1–19. https://doi.org/10.1016/j.actbio.2024.08.037

[7] Liang J, Yang B, Zhou X, Han Q, Zou J, Cheng L. Stimuli-responsive drug delivery systems for head and neck cancer therapy. Drug Delivery. 2021; 28: 272–284. https://doi.org/10.1080/10717544.2021.1876182

[8] Li Z, Song N, Yang YW. Stimuli-responsive drug-delivery sys-

tems based on supramolecular nanovalves. Matter. 2019; 1: 345–368. https://doi.org/10.1016/j.matt.2019.05.019
[9] Naziris N, Pippa N, Pispas S, Demetzos C. Stimuli-responsive drug delivery nanosystems: From bench to clinic. Current Nanomedicine. 2016; 6: 166–185. https://doi.org/10.2174/2468187306666160712232449
[10] Taghizadeh B, Taranejoo S, Monemian SA, Salehi Moghaddam Z, Daliri K, Derakhshankhah H, et al. Classification of stimuli-responsive polymers as anticancer drug delivery systems. Drug Delivery. 2015; 22: 145–155. https://doi.org/10.3109/10717544.2014.887157
[11] Ghezzi M, Pescina S, Padula C, Santi P, Del Favero E, Cantù L, et al. Polymeric micelles in drug delivery: An insight of the techniques for their characterization and assessment in biorelevant conditions. Journal of Controlled Release: Official Journal of the Controlled Release Society. 2021; 332: 312–336. https://doi.org/10.1016/j.jconrel.2021.02.031
[12] Jiang L, Zheng R, Zeng N, Wu C, Su H. *In situ* self-assembly of amphiphilic dextran micelles and superparamagnetic iron oxide nanoparticle-loading as magnetic resonance imaging contrast agents. Regenerative Biomaterials. 2023; 10: rbac096. https://doi.org/10.1093/rb/rbac096
[13] Kulthe SS, Choudhari YM, Inamdar NN, Mourya VK. Polymeric micelles: Authoritative aspects for drug delivery. Designed Monomers and Polymers. 2012; 15: 465–521. https://doi.org/10.1080/1385772X.2012.688328
[14] Wei HX, Liu MH, Wang TY, Shih MH, Yu J, Yeh YC. Fabrication of pH- and Ultrasound-Responsive Polymeric Micelles: The Effect of Amphiphilic Block Copolymers with Different Hydrophilic/Hydrophobic Block Ratios for Self-Assembly and Controlled Drug Release. Biomacromolecules. 2025; 26: 2116–2130. https://doi.org/10.1021/acs.biomac.4c01202
[15] Assiri AA, Glover K, Mishra D, Waite D, Vora LK, Thakur RRS. Block copolymer micelles as ocular drug delivery systems. Drug Discovery Today. 2024; 29: 104098. https://doi.org/10.1016/j.drudis.2024.104098
[16] Kim TH, Alle M, Park SC, Zhao F, Long W, Samala S, et al. Self-assembly prepared using an ion pair of poly(ethylene imine) and (phenylthio)acetic acid as a drug carrier for oxidation, temperature, and NIR-responsive release. Chemical Engineering Journal. 2021; 415: 128954. https://doi.org/10.1016/j.cej.2021.128954
[17] Hwang JS, Kim JC. Reduction and temperature responsive ion pair self-assembled nanoparticles composed of poly(allylamine) and α-lipoic acid. Colloid and Polymer Science. 2026; 304: 79–92. https://doi.org/10.1007/s00396-025-05512-6
[18] Danielsen SPO, Panyukov S, Rubinstein M. Ion Pairing and the Structure of Gel Coacervates. Macromolecules. 2020; 53: 9420–9442. https://doi.org/10.1021/acs.macromol.0c01360
[19] Antila HS, Sammalkorpi M. Polyelectrolyte decomplexation via addition of salt: charge correlation driven zipper. The Journal of Physical Chemistry. B. 2014; 118: 3226–3234. https://doi.org/10.1021/jp4124293
[20] Ogawa K. Effects of salt on intermolecular polyelectrolyte complexes formation between cationic microgel and polyanion. Advances in Colloid and Interface Science. 2015; 226: 115–121. https://doi.org/10.1016/j.cis.2015.09.005
[21] Sharma G, Wangpimool K, George Joy J, Sharma AR, Son HK, Kim S, et al. A Facile Approach To Develop Ion Pair Micelles Satellited Freshly Derived Neutrophils For Targeted Tumor Therapy. Advanced Healthcare Materials. 2025; 14: e2404105. https://doi.org/10.1002/adhm.202404105
[22] Baker LB. Sweating Rate and Sweat Sodium Concentration in Athletes: A Review of Methodology and Intra/Interindividual Variability. Sports Medicine (Auckland, N.Z.). 2017; 47: 111–128. https://doi.org/10.1007/s40279-017-0691-5
[23] Minsart M, Van Vlierberghe S, Dubruel P, Mignon A. Commercial wound dressings for the treatment of exuding wounds: an in-depth physico-chemical comparative study. Burns & Trauma. 2022; 10: tkac024. https://doi.org/10.1093/burnst/tkac024
[24] Sun L, Hou Y, Xiao Q, Du Y. Association of serum sodium and risk of all-cause mortality in patients with chronic kidney disease: A meta-analysis and sysematic review. Scientific Reports. 2017; 7: 15949. https://doi.org/10.1038/s41598-017-16242-3
[25] Hamroun A, Pekar JD, Lionet A, Ghulam A, Maboudou P, Mercier A, et al. Ionized calcium: analytical challenges and clinical relevance. Journal of Laboratory and Precision Medicine. 2020; 5: 22. https://doi.org/10.21037/jlpm-20-60
[26] Kutus B, Wagner K, Wagner M, Hunger J. Ion-pairing equilibria and kinetics of dimethyl phosphate: A model for counter-ion binding to the phosphate backbone of nucleic acids. Journal of Molecular Liquids. 2022; 363: 119868. https://doi.org/10.1016/j.molliq.2022.119868
[27] Braide T, Manoj Lalwani S, Eneh CI, Lutkenhaus JL. Divalent cation effects in the glass transition of poly(diallyldimethylammonium)-poly(styrene sulfonate) polyelectrolyte complexes. Soft Matter. 2024; 20: 9631–9641. https://doi.org/10.1039/d4sm00856a
[28] Iyer D, Syed VMS, Srivastava S. Influence of divalent ions on composition and viscoelasticity of polyelectrolyte complexes. Journal of Polymer Science. 2021; 59: 2895–2904. https://doi.org/10.1002/pol.20210668
[29] Gindele MB, Malaszuk KK, Peter C, Gebauer D. On the Binding Mechanisms of Calcium Ions to Polycarboxylates: Effects of Molecular Weight, Side Chain, and Backbone Chemistry. Langmuir: the ACS Journal of Surfaces and Colloids. 2022; 38: 14409–14421. https://doi.org/10.1021/acs.langmuir.2c01662
[30] Mantha S, Glisman A, Yu D, Wasserman EP, Backer S, Wang ZG. Adsorption Isotherm and Mechanism of Ca^{2+} Binding to Polyelectrolyte. Langmuir: the ACS Journal of Surfaces and Colloids. 2024; 40: 6212–6219. https://doi.org/10.1021/acs.langmuir.3c03640
[31] Rodriguez-Loya J, Lerma M, Gardea-Torresdey JL. Dynamic Light Scattering and Its Application to Control Nanoparticle Aggregation in Colloidal Systems: A Review. Micromachines. 2024; 15: 24. https://doi.org/10.3390/mi15010024
[32] Anzini P, Redoglio D, Rocco M, Masciocchi N, Ferri F. Light Scattering and Turbidimetry Techniques for the Characterization of Nanoparticles and Nanostructured Networks. Nanomaterials (Basel, Switzerland). 2022; 12: 2214. https://doi.org/10.3390/nano12132214
[33] Iwata N, Koike T, Tokuhiro K, Sato R, Furumi S. Colloidal Photonic Crystals of Reusable Hydrogel Microparticles for Sensor and Laser Applications. ACS Applied Materials & Interfaces. 2021; 13: 57893–57907. https://doi.org/10.1021/acsami.1c16500
[34] Le Roux S, Roché M, Cantat I, Saint-Jalmes A. Soluble surfactant spreading: How the amphiphilicity sets the Marangoni hydrodynamics. Physical Review. E. 2016; 93: 013107. https://doi.org/10.1103/PhysRevE.93.013107
[35] Perinelli DR, Cespi M, Lorusso N, Palmieri GF, Bonacucina G, Blasi P. Surfactant Self-Assembling and Critical Micelle Concentration: One Approach Fits All? Langmuir: the ACS Journal of Surfaces and Colloids. 2020; 36: 5745–5753. https://doi.org/10.1021/acs.langmuir.0c00420
[36] Mukherjee I, Moulik SP, Rakshit AK. Tensiometric determination of Gibbs surface excess and micelle point: a critical revisit. Journal of Colloid and Interface Science. 2013; 394: 329–336. https://doi.org/10.1016/j.jcis.2012.12.004
[37] Yu D, Huang X, Deng M, Lin Y, Jiang L, Huang J, et al. Effects of inorganic and organic salts on aggregation behavior of cationic gemini surfactants. The Journal of Physical Chemistry. B. 2010;

114: 14955–14964. https://doi.org/10.1021/jp106031d
[38] Ren ZH. Mechanism of the salt effect on micellization of an aminosulfonate amphoteric surfactant. Industrial & Engineering Chemistry Research. 2015; 54: 9683–9688. https://doi.org/10.1021/acs.iecr.5b02169
[39] Katana B, Takács D, Csapó E, Szabó T, Jamnik A, Szilagyi I. Ion Specific Effects on the Stability of Halloysite Nanotube Colloids-Inorganic Salts versus Ionic Liquids. The Journal of Physical Chemistry. B. 2020; 124: 9757–9765. https://doi.org/10.1021/acs.jpcb.0c07885
[40] Kriegseis S, Vogl AY, Aretz L, Tonnesen T, Telle R. Zeta potential and long-term stability correlation of carbon-based suspensions for material jetting. Open Ceramics. 2020; 4: 100037. https://doi.org/10.1016/j.oceram.2020.100037
[41] Farooq S, Habib M, Cardozo O, Ullah K, Pandey AK, Said Z. Exploring the impact of particle stability, size, and morphology on nanofluid thermal conductivity: A comprehensive review for energy applications. Advances in Colloid and Interface Science. 2025; 341: 103495. https://doi.org/10.1016/j.cis.2025.103495
[42] Harris JR, Roos C, Djalali R, Rheingans O, Maskos M, Schmidt M. Application of the negative staining technique to both aqueous and organic solvent solutions of polymer particles. Micron. 1999; 30: 289–298. https://doi.org/10.1016/S0968-4328(99)00034-7
[43] Nigro V, Angelini R, Rosi B, Bertoldo M, Buratti E, Casciardi S, et al. Study of network composition in interpenetrating polymer networks of poly(N isopropylacrylamide) microgels: The role of poly(acrylic acid). Journal of Colloid and Interface Science. 2019; 545: 210–219. https://doi.org/10.1016/j.jcis.2019.03.004